Effect of One-Coordinated Atoms on the Electronic and Optical Properties of ZnSe Clusters

Xiaolin Wang, Yongcheng Zhu, Mei Liu, Gang Jiang, Gao-Lei Hou,* Meng Zhang,* and Kui Yu*
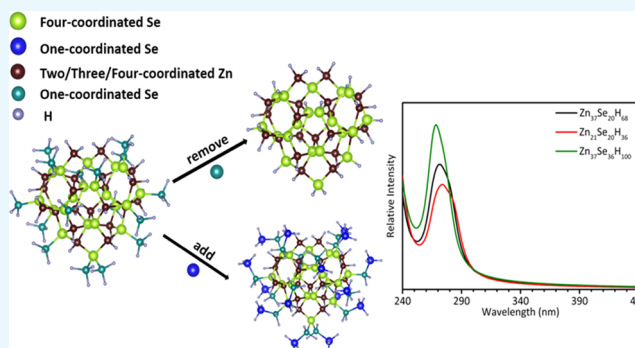
Read Online

ACCESS | Metrics & More | Article Recommendations | SI Supporting Information

ABSTRACT: To understand the influence of one-coordinated Zn and Se atoms on the structures, electronic, and optical properties of ZnSe clusters, we investigate the $Zn_{37}Se_{20}$ clusters employing first-principles theoretical calculations. The $Zn_{37}Se_{20}$ cluster, constructed from the InP nanocrystal structure, possesses a $Zn_{21}Se_{20}$ core and 16 one-coordinated surface atoms. The effect of one-coordinated atoms is studied by adding or removing one-coordinated atoms of the $Zn_{37}Se_{20}$ cluster. The calculations show that the modifications of one-coordinated atoms change slightly the coordination states and bond lengths of the atoms on the cluster surface. The clusters with the same core structure and different amounts of one-coordinated atoms have similar optical spectra, suggesting the importance of the cluster core structure in their optical properties.

INTRODUCTION

Colloidal semiconductor quantum dots (QDs) possess unique optical,[1] magnetic,[2] and catalytic[3] properties that are different from bulk materials due to strong quantum confinement of QDs. The properties of QDs can be finely tuned by changing their surface passivation,[4−6] shape,[7] and size.[8,9] The high-quality synthesis of QDs ensures their practical applications in multiple fields, such as biolabeling,[10] solar cells,[11,12] and laser.[13]

Magic-size clusters (MSCs) are a type of nanoparticles with specific numbers of atoms, which usually form along with the nucleation and growth of QDs. The investigations of MSCs are of essential significance to the understanding of the formation mechanism of QDs.[14,15] MSCs have attracted much attention due to their high stability with typical sizes in the range of 1−3 nm.[16,17] Investigation of MSCs, in particular, their atomic structures and optical properties, is crucial for understanding their good performance in nanodevices.[18] Various structures of MSCs, including core−cage $(CdSe)_n$ (n = 13, 33, and 34),[19] tetrahedral $Cd_{35}Se_{20}X_{30}L_{30}$,[20] and $In_{37}P_{20}(OOCCH_2Ph)_{51}$ nanoclusters,[21] have been reported. Recently, Robinson and co-workers[22] investigated the CdS MSC with an absorption maximum at about 311 nm (MSC-311), which has been assumed to be of the InP nanocrystal structure.[21] The pair distribution function (PDF) of CdS based on the single crystal of $In_{37}P_{20}(OOCCH_2Ph)_{51}$ coincides with the PDF of CdS MSC-311.[23] These results suggest that the $In_{37}P_{20}$ structure may be applicable to the II−VI metal chalcogenide cluster systems, such as the ZnSe cluster. We are inspired to investigate whether the ZnSe MSC with the absorption

maximum at 299 nm (MSC-299)[24] found previously also has a similar structure to that of InP MSC. The removal and/or substitution of one-coordinated In atoms with three dangling bonds in InP MSCs showed their influence on the structure and optical properties of InP clusters.[25−27] Considering that the one-coordinated atoms are on the cluster surface, an in-depth understanding of the optical and electronic nature of clusters[28] is critical for exploring their formation mechanisms.[29] Hence, it will be interesting to investigate at a molecular level how the atoms in different coordination states influence the optical properties of the ZnSe cluster.

In this work, we choose the $Zn_{37}Se_{20}$ cluster, which is constructed based on the atomic structure of InP MSC, as a model to investigate the influence of one-coordinated atoms on the property of the cluster. This model has one $Zn_{21}Se_{20}$ core and 16 one-coordinated Zn atoms. By removing Zn atoms and adding Se atoms, we construct the respective $Zn_{37−n}Se_{20}$ (n = 1−16) and $Zn_{37}Se_{20+m}$ (m = 1−16) clusters and investigate their structures, stabilities, and optical properties.

■ RESULTS AND DISCUSSION

Structure of $Zn_{37}Se_{20}H_{68}$. Based on the InP nanocluster structure,[21] the $Zn_{37}Se_{20}$ model cluster was built by replacing In and P atoms with Zn and Se, respectively. The optimized structure of $Zn_{37}Se_{20}$ with 68 pseudo hydrogens is shown in Figure 1, and it can be seen that it largely maintains the
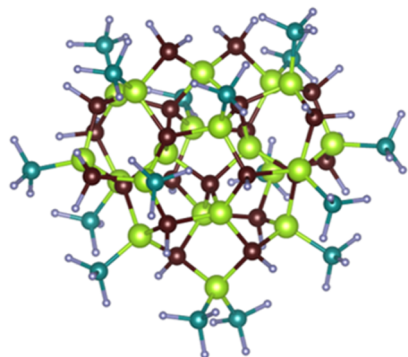

Figure 1. Optimized structure of the $Zn_{37}Se_{20}$ cluster with the dangling bonds saturated with 68 pseudo hydrogens. The different colors in the model represent H (silver), Se (green), and Zn atoms in either one-coordinated state (cyan) or other coordinated states (brown).

structural features of InP MSC. The structure has a pseudo-C2 symmetry, with Se and Zn atoms symmetrically distributed along the C2 axis.[25] The $Zn_{37}Se_{20}$ structure contains six-membered rings formed by three Se and three Zn atoms (Figure S1) and tetrahedrons by one Se and four neighboring Zn atoms. This is similar to the previously reported zinc blende and wurtzite structures.[30] Specifically, in the absence of pseudo hydrogen atoms, the $Zn_{37}Se_{20}$ structure has 20 four-coordinated Se atoms, with each atom bonded to four Zn atoms, 7 four-coordinated Zn atoms, with each atom bonded to four Se atoms, 8 three-coordinated Zn atoms, with each atom bonded to three Se atoms, 6 two-coordinated Zn atoms, with each atom bonded to two Se atoms, and 16 one-coordinated Zn atoms, with each atom bonded to one Se atoms (Figures S1 and S2 and Table S1). The three-, two-, and one-coordinated Zn atoms need to be saturated with pseudo hydrogen atoms to result in the $Zn_{37}Se_{20}H_{68}$ structure prior to calculation. Moreover, it has been reported that the one-

coordinated atoms more readily dissociate than those in other coordination states.[6]

The electron density distribution of $Zn_{37}Se_{20}H_{68}$ is explored via the electron localization function (ELF). As shown in Figure S3, the ELF value of Se atoms is about 0.8, while that of Zn atoms is much lower, suggesting a strong localization of electrons around Se atoms[31] and a relatively low electron density of Zn atoms. These results may suggest a charge transfer from Zn to Se atoms, which is further supported by the charge density difference (CDD) pattern (Figure S4). The charges of pseudo hydrogens are localized at the passivated sites, and no charge transfer is observed between pseudo hydrogens in different sites, consistent with the previous findings.[32] Meanwhile, the Bader charge analysis of the $Zn_{37}Se_{20}H_{68}$ cluster suggests that each Se atom acquires 0.86 electrons from the surrounding four Zn atoms (Table S1).

Structures of $Zn_{37-n}Se_{20}$ (n = 0−16) and $Zn_{37}Se_{20+m}$ (m = 1−16) Nanoclusters. The one-coordinated atoms are generally chemically active compared to the two-/three-coordinated atoms. To understand the effect of one-coordinated atoms, we modify the $Zn_{37}Se_{20}$ cluster structure by either removing the one-coordinated Zn atoms or adding Se atoms to the one-coordinated Zn atoms. It is noteworthy that we do not modify the Se atoms of the $Zn_{37}Se_{20}$ structure as they are all saturated in the four-coordinated state.

The $Zn_{37-n}Se_{20}$ (n = 1−16) (Figures 2 and S5) and $Zn_{37}Se_{20+m}$ (m = 1−16) clusters (Figures 3 and S6) constructed have similar geometries but slightly different coordination states and bond lengths for the surface atoms. It is noted that the coordination states of the surface atoms changed upon removing or adding certain atoms. For example, the Se atom becomes three-coordinated upon removing the corresponding one-coordinated Zn atom, while the one-coordinated Zn atom becomes two-coordinated upon adding one Se atom.

Table 1 summarizes the average bond lengths of Se−Zn and those of the three-coordinated Se atoms binding with three neighboring Zn atoms (Se(3)−Zn) and the one-coordinated Se atoms binding with one Zn atom (Se(1)−Zn). The average bond lengths for two- and four-coordinated Se binding with Zn atoms (Se(2)−Zn, Se(4)−Zn) are shown in Table S2. In general, the average Se−Zn bond length changes little at about 2.474 Å upon the modifications. In addition, the Se(1)−Zn bond lengths are the shortest, while those of Se(3)−Zn and
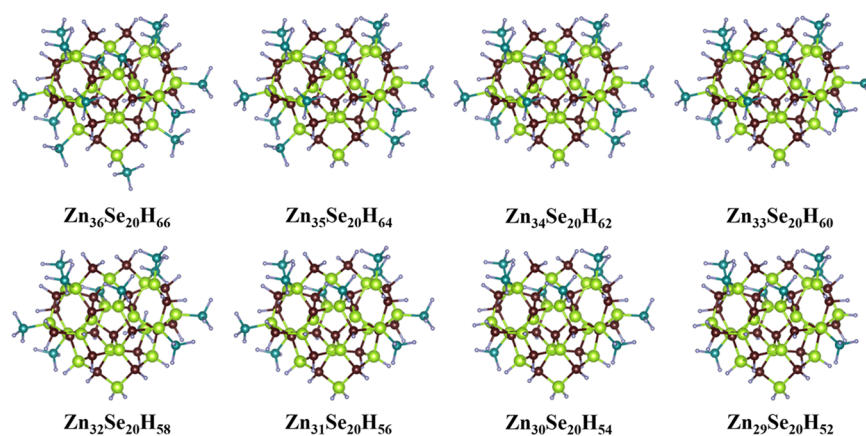

| $Zn_{36}Se_{20}H_{66}$ | $Zn_{35}Se_{20}H_{64}$ | $Zn_{34}Se_{20}H_{62}$ | $Zn_{33}Se_{20}H_{60}$ |

| $Zn_{32}Se_{20}H_{58}$ | $Zn_{31}Se_{20}H_{56}$ | $Zn_{30}Se_{20}H_{54}$ | $Zn_{29}Se_{20}H_{52}$ |

Figure 2. Optimized structures of the $Zn_{37-n}Se_{20}$ (n = 1−8) clusters with the dangling bonds saturated by pseudo hydrogens. The different colors in the model represent H (silver), Se (green), and Zn atoms in either one-coordinated state (cyan) or other coordinated states (brown).
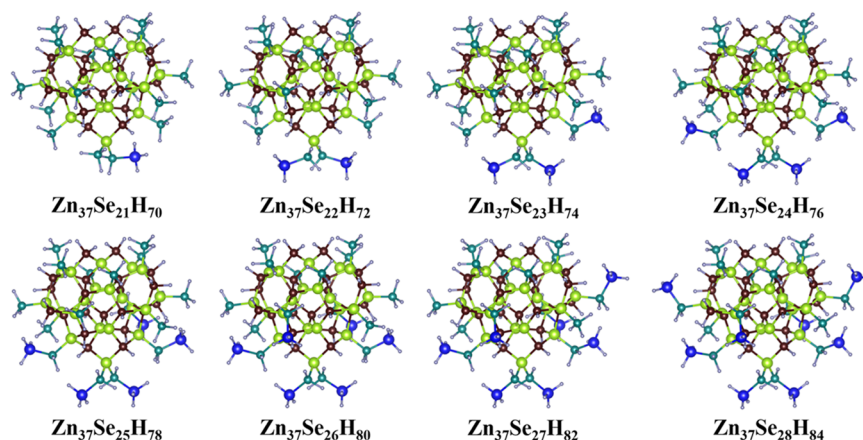
Figure 3. Optimized structures of the $Zn_{37}Se_{20+m}$ ($m = 1-8$) clusters with the dangling bonds saturated by pseudo hydrogens. The different colors in the model represent H (silver) and Se atoms in four- (green) or one-coordinated state (blue) and Zn atoms in either one-coordinated state (cyan) or other coordinated states (brown).

Table 1. Average Bond Lengths of Se−Zn, Se(3)−Zn, and Se (1)−Zn in $Zn_{37-n}Se_{20}$ ($n = 0-16$) and $Zn_{37}Se_{20+m}$ ($m = 1-16$) Clusters

clusters	average bond length of Se−Zn (Å)	average Se (3)−Zn bond length (Å)	clusters	average bond length of Se−Zn (Å)	average Se (1)−Zn bond length (Å)
$Zn_{37}Se_{20}H_{68}$	2.474				
$Zn_{36}Se_{20}H_{66}$	2.474	2.456	$Zn_{37}Se_{21}H_{70}$	2.474	2.399
$Zn_{35}Se_{20}H_{64}$	2.474		$Zn_{37}Se_{22}H_{72}$	2.473	2.408
$Zn_{34}Se_{20}H_{62}$	2.474	2.482	$Zn_{37}Se_{23}H_{74}$	2.473	2.405
$Zn_{33}Se_{20}H_{60}$	2.474	2.483	$Zn_{37}Se_{24}H_{76}$	2.472	2.404
$Zn_{32}Se_{20}H_{58}$	2.474	2.478	$Zn_{37}Se_{25}H_{78}$	2.472	2.406
$Zn_{31}Se_{20}H_{56}$	2.474	2.475	$Zn_{37}Se_{26}H_{80}$	2.471	2.406
$Zn_{30}Se_{20}H_{54}$	2.474	2.475	$Zn_{37}Se_{27}H_{82}$	2.471	2.407
$Zn_{29}Se_{20}H_{52}$	2.474	2.475	$Zn_{37}Se_{28}H_{84}$	2.470	2.406
$Zn_{28}Se_{20}H_{50}$	2.474	2.474	$Zn_{37}Se_{29}H_{86}$	2.470	2.408
$Zn_{27}Se_{20}H_{48}$	2.474	2.473	$Zn_{37}Se_{30}H_{88}$	2.469	2.409
$Zn_{26}Se_{20}H_{46}$	2.474	2.474	$Zn_{37}Se_{31}H_{90}$	2.469	2.410
$Zn_{25}Se_{20}H_{44}$	2.474	2.474	$Zn_{37}Se_{32}H_{92}$	2.469	2.411
$Zn_{24}Se_{20}H_{42}$	2.474	2.474	$Zn_{37}Se_{33}H_{94}$	2.469	2.412
$Zn_{23}Se_{20}H_{40}$	2.475	2.475	$Zn_{37}Se_{34}H_{96}$	2.469	2.414
$Zn_{22}Se_{20}H_{38}$	2.475	2.475	$Zn_{37}Se_{35}H_{98}$	2.468	2.412
$Zn_{21}Se_{20}H_{36}$	2.475	2.476	$Zn_{37}Se_{36}H_{100}$	2.468	2.412

Se(4)−Zn are the longest and are similar to each other. It appears that the bonds with the Se atom in a lower coordinated state exhibit shorter lengths, which agrees well with a previous study about the ZnSe nanoclusters.[33]

Relative Stabilities. We computed the second difference in energy ($\Delta_2 E$), the binding energy (E_b), and the highest occupied molecular orbital (HOMO) and lowest unoccupied molecular orbital (LUMO) energy gap (ΔE_{HL}) to evaluate the stability of $Zn_{37-n}Se_{20}$ ($n = 0-16$) and $Zn_{37}Se_{20+m}$ ($m = 0-16$) clusters.

The $\Delta_2 E$ reflects the stability of a cluster with respect to its neighbors (Figure 4a). The calculated $\Delta_2 E$ values of the $Zn_{37-n}Se_{20}$ ($n = 0-16$) and $Zn_{37}Se_{20+m}$ ($m = 0-16$) clusters show an oscillation behavior. It is noted that $Zn_{35}Se_{20}$, $Zn_{32}Se_{20}$, $Zn_{29}Se_{20}$, $Zn_{27}Se_{20}$, and $Zn_{24}Se_{20}$ clusters exhibit high $\Delta_2 E$ values, suggesting that they are relatively more stable than their neighbors of $Zn_{37-n}Se_{20}$ ($n = 0-16$) clusters. Similarly, the $Zn_{37}Se_{22}$, $Zn_{37}Se_{25}$, $Zn_{37}Se_{29}$, $Zn_{37}Se_{32}$, and
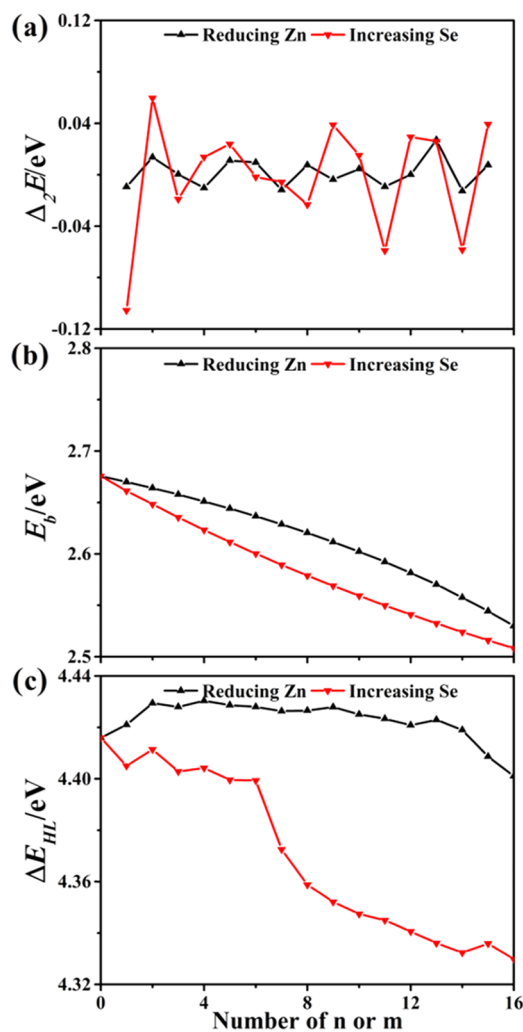

Figure 4. Second-order energy difference $\Delta_2 E$ (a), average binding energies E_b (b), and HOMO−LUMO gap ΔE_{HL} (c) of $Zn_{37-n}Se_{20}$ ($n = 0-16$) and $Zn_{37}Se_{20+m}$ ($m = 0-16$) clusters saturated with pseudo hydrogens.

$Zn_{37}Se_{35}$ clusters of the $Zn_{37}Se_{20+m}$ ($m = 0-16$) clusters have relatively high stabilities than their neighbors.
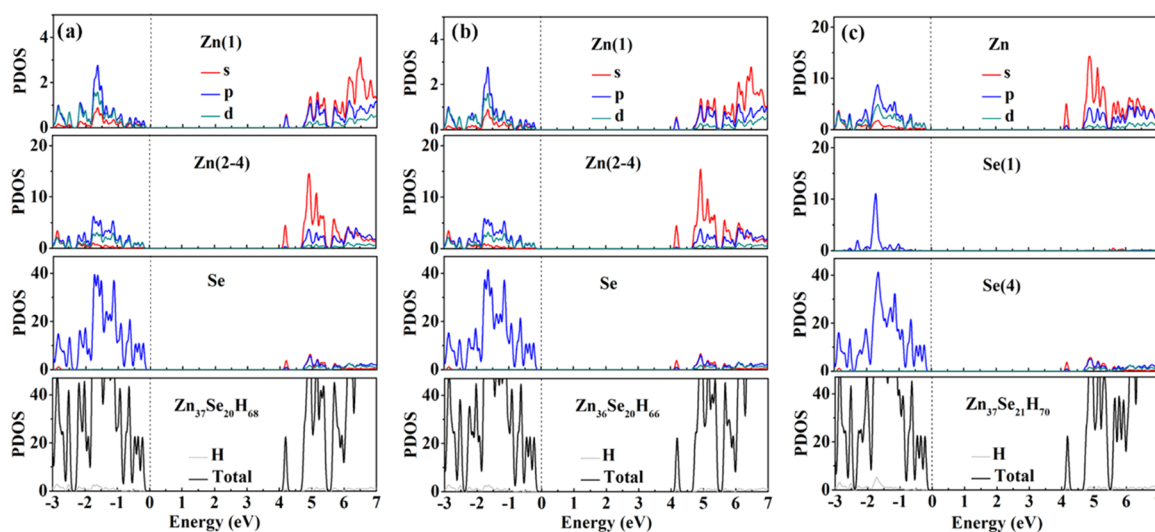
Figure 5. Projected density of states (PDOSs) of $Zn_{37}Se_{20}H_{68}$ (a), $Zn_{36}Se_{20}H_{66}$ (b), and $Zn_{37}Se_{21}H_{70}$ (c). In the figure, (2–4) = two-, three-, and four-coordinated atoms, (1) = one-coordinated atoms, and (4) = four-coordinated atoms. The Se atoms are all in four-coordinated states except that the added Se atoms are in one-coordinated states in $Zn_{37}Se_{20+m}$ (m = 1–16) clusters. Note that Fermi energy is set to zero.

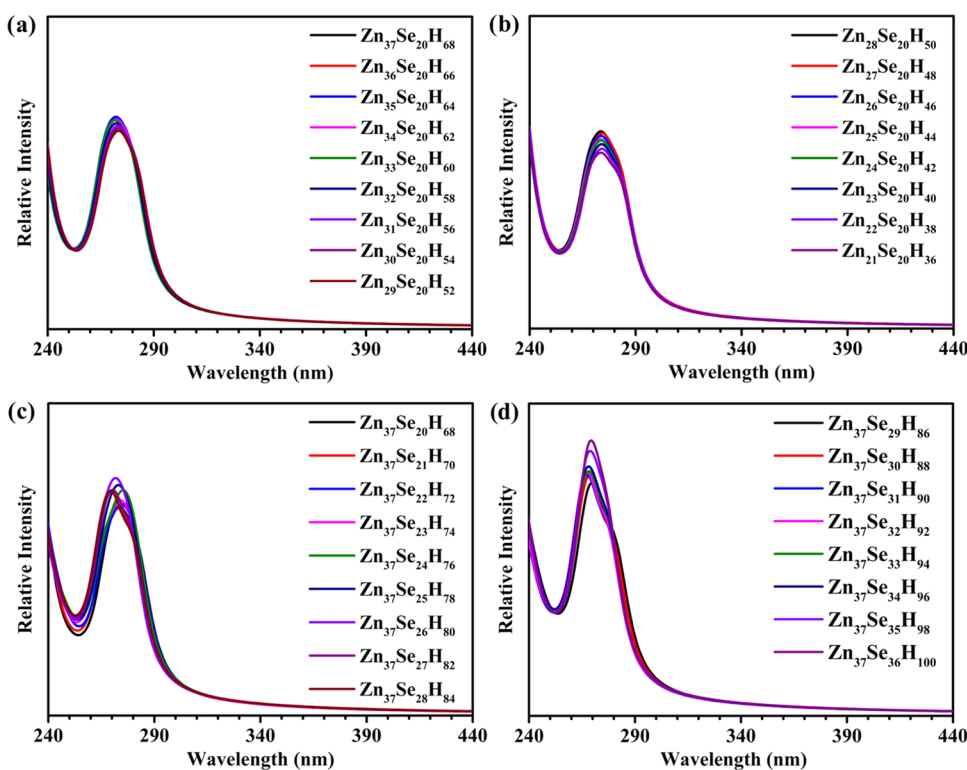**Figure 6.** Calculated absorption spectra of (a) $Zn_{37-n}Se_{20}$ (n = 0–8), (b) $Zn_{37-n}Se_{20}$ (n = 9–16), (c) $Zn_{37}Se_{20+m}$ (m = 0–8), and (d) $Zn_{37}Se_{20+m}$ (m = 9–16) clusters passivated by pseudo hydrogens.

The E_b represents the stability of one species relative to their constituent individual atoms, and Figure 4b shows that E_b decreases with the decrease of the number of one-coordinated Zn atoms and with the increase of the number of one-coordinated Se atoms.

The ΔE_{HL} is closely related to the energy required by the transfer of electrons from HOMO to LUMO.[34,35] The variation of ΔE_{HL} as a function of the number of one-coordinated Zn and Se atoms for $Zn_{37-n}Se_{20}$ (n = 0–16) and $Zn_{37}Se_{20+m}$ (m = 0–16) clusters is presented in Figure 4c. The ΔE_{HL} values increase slightly first with the decreasing number

of one-coordinated Zn atoms of $Zn_{37-n}Se_{20}$ (n = 0–16), reaching the maximum when n = 4. Upon further decreasing the one-coordinated Zn atoms, the corresponding ΔE_{HL} values decrease gradually, which indicates a quite stable nature of the $Zn_{33}Se_{20}$ cluster. However, the ΔE_{HL} values of the $Zn_{37}Se_{20+m}$ (m = 0–16) clusters have a decreasing trend, which is similar to the previous work on CdSe QDs.[28] It is noteworthy that the differences between the maximum and minimum ΔE_{HL} for $Zn_{37-n}Se_{20}$ (n = 0–16) and $Zn_{37}Se_{20+m}$ (m = 0–16) are 0.03 and 0.08 eV, respectively. Such small variations suggest that

one-coordinated atoms only slightly perturb the molecular orbital energy levels of the studied clusters.

Electronic and Optical Properties. To investigate the effect of the one-coordinated Zn and Se atoms on the electronic structures, Figure 5 presents the projected density of states (PDOSs) of three selected clusters, which are $Zn_{37}Se_{20}H_{68}$, $Zn_{36}Se_{20}H_{66}$, and $Zn_{37}Se_{21}H_{70}$ (see Figures S7 to S16 for the PDOS plots of all of the studied clusters).

For $Zn_{37-n}Se_{20}$ ($n = 0-16$) and $Zn_{37}Se_{20+m}$ ($m = 1-16$) clusters, their HOMOs mainly arise from Se 4p orbitals and are close in energy with the other occupied orbitals and their LUMOs are predominantly contributed by Zn 4s and Se 4s orbitals. The LUMOs are separated from the higher unoccupied orbitals with differences of up to ∼0.5 eV, comparable with a previously published theoretical work.[36]

The one-coordinated Zn atoms have little contribution to the HOMO and LUMO of those clusters, while the states of one-coordinated Se atoms do not appear near the Fermi level region, merely influencing the optical properties of the studied clusters. The plots also show that the HOMO and LUMO are primarily contributed by the atoms in non-one-coordinated states that are only slightly perturbed by the one-coordinated atoms. That explains why the DOS near the Fermi energy level looks similar for all of the $Zn_{37-n}Se_{20}$ ($n = 0-16$) and $Zn_{37}Se_{20+m}$ ($m = 1-16$) clusters.

The calculated optical absorption spectra of $Zn_{37-n}Se_{20}$ ($n = 0-16$) and $Zn_{37}Se_{20+m}$ ($m = 0-16$) are shown in Figure 6. Figure 6a,b shows that there is the only a minor influence of one-coordinated Zn atoms on the absorption spectra regarding both the peak shape and maxima, and only 3 nm red-shifts are found when the value of n increases from 0 to 16. Similarly, adding Se atoms to $Zn_{37}Se_{20}$ also does not affect much the optical absorption spectra of the clusters (Figure 6c,d). A gradual red-shift with a maximum of 7 nm is found when 16 Se atoms are added. The comparison suggests that neither one-coordinated Zn nor one-coordinated Se atoms perturb much the absorption behavior of the clusters, emphasizing the importance of the electron excitations of the cluster core. That is in line with the finding of the PDOS plots in Figure 5. In addition, it is noted that the calculated absorption spectra of $Zn_{37}Se_{20}$, $Zn_{37-n}Se_{20}$ ($n = 1-16$), and $Zn_{37}Se_{20+m}$ ($m = 1-16$) are all similar to that of ZnSe MSC-299 measured experimentally (see Figures 6 and S17). However, understanding the atomic structure of ZnSe MSC-299 is still not trivial, warranting further efforts.

CONCLUSIONS

In summary, we systematically investigate the effect of one-coordinated atoms on the properties of the ZnSe clusters using first-principles theoretical calculations. The addition or removal of one-coordinated atoms changes the coordination states and the local bond lengths of the remaining surface atoms. However, the plots of PDOS, HOMO, and LUMO show that the modifications only affect slightly the states close to the Fermi level region. The states near the edges of the band gap are mainly attributed to the interior Zn and Se atoms, emphasizing the importance of the cluster core. The calculated absorption spectra of the ZnSe clusters further confirm that the electron excitation of the cluster core is critical for their optical properties. This work provides an in-depth understanding of the structures and optical properties of the ZnSe magic-size clusters.

Computational Methods. The geometric and electronic structures and optical properties are calculated using density functional theory (DFT) with the Kohn−Sham (KS) representation[37] implemented in Vienna Ab initio Simulation Package (VASP).[38] Compared with other first-principles software, such as Amsterdam density functional (ADF)[39] and Gaussian code,[40] VASP has high efficiency in algorithm optimization and good stability. There are dangling bonds on the surface of the ZnSe clusters, which are commonly passivated with chemical ligands after synthesis.[24] Due to the large quantities of atoms in these ligands have, it is difficult to calculate the corresponding structures. Certain ligands with simple structures, such as pseudo hydrogen atoms,[41] may be used to simplify the cluster structure for theoretical studies.[42] Pseudo hydrogen is a type of virtual ligand that exhibits fractional charge, and it has been reported to be able to remove the band gap states introduced by the surface dangling bonds,[41−43] leading to results that match well with the experimental data.[44] Therefore, it may be a good candidate to simplify the structure of ZnSe clusters for calculations. For group II−VI clusters, the surface atom with Z formal valence may be passivated via pseudo hydrogen atoms with fractional charge $\alpha = (8-Z)/4$.[42,45] Thus, in this work, the Zn and Se atoms with respective formal valences of 2 and 6 are saturated with pseudo hydrogen atoms with charges of 1.5 and 0.5e, respectively.[46] The Zn and Se potentials are simulated by the projector-potential plane wave[47] method from the VASP potential library. The valence electrons of Zn and Se atoms are treated as $3d^{10}4s^2$ and $4s^24p^4$, respectively. The cutoff energy is 370 eV in all calculations. The cell size is set as 30 Å × 30 Å × 30 Å to eliminate the interactions between periodic images of the cluster.[48] We set only one γ point in the calculations.[30,49,50] The convergence of the total energies is set as 10^{-6} eV for structure optimization. The Heyd−Scuseria−Ernzerhof (HSE06) provides part of the precise exchange functional, and its calculated gap value is close to the one obtained by the experiment.[51,52] HSE06 has previously been shown to be reliable for calculating the properties of molecules and clusters.[31,53] Thus, the electronic structure and optical properties are calculated with HSE06 functional incorporated into the VASP code. The electron localization function (ELF) is employed to analyze the distribution of electrons and the property related to electron localization.[54] The ELF value is between 0 and 1, with the value close to 1 representing a strong localization of electrons.[55] The ELF was calculated using VASP, and its visualization was performed using the VESTA code.[56] In addition, the charge transfer in the clusters was estimated via charge density difference (CDD) and the Bader charge analysis.[57,58]

The CDD is defined as follows

$$\text{CDD} = \rho_{Zn_{37}Se_{20}H_{68}} - \rho_{Zn} - \rho_{Se} - \rho_H \tag{1}$$

where $\rho_{Zn_{37}Se_{20}H_{68}}$, ρ_{Zn}, ρ_{Se}, and ρ_H are the charge densities of $Zn_{37}Se_{20}H_{68}$, the noninteracting Zn, Se, and H atoms, respectively.

The second difference in energy is defined as

$$\Delta_2 E(n) = E(Zn_{37-(n+1)}Se_{20}H^*_{x-2})$$
$$+ E(Zn_{37-(n-1)}Se_{20}H^*_{x+2}) -$$
$$2E(Zn_{37-n}Se_{20}H^*_x) \tag{2}$$

$$\Delta_2 E(m) = E(\text{Zn}_{37}\text{Se}_{20+(m+1)}\text{H}^*_{y+2})$$
$$+ E(\text{Zn}_{37}\text{Se}_{20+(m-1)}\text{H}^*_{y-2}) - 2$$
$$E(\text{Zn}_{37}\text{Se}_{20+m}\text{H}^*_y) \qquad (3)$$

where $E(\text{Zn}_{37-n}\text{Se}_{20}\text{H}_x)$ is the total energy of $\text{Zn}_{37-n}\text{Se}_{20}\text{H}_x$ and $E(\text{Zn}_{37-(n+1)}\text{Se}_{20}\text{H}_{x-1})$ and $E(\text{Zn}_{37-(n-1)}\text{Se}_{20}\text{H}_{x+1})$ are the energies of its neighbors.

The average binding energy per atom (E_b) is calculated by

$$E_b = [nE(\text{Zn}) + mE(\text{Se}) + kE(\text{H}^{1.5e}) + lE(\text{H}^{0.5e})$$
$$- E(\text{Zn}_n\text{Se}_m\text{H}^*_{k+l})]/(n + m + k + l) \qquad (4)$$

where $E(\text{Zn})$, $E(\text{Se})$, $E(\text{H}^{1.5e})$, and $E(\text{H}^{0.5e})$ are the energies of a single Zn, Se, pseudo H (with charge 1.5e), and pseudo H (with charge 0.5e) atoms in $\text{Zn}_n\text{Se}_m\text{H}_{k+l}$.

■ ASSOCIATED CONTENT

ⓢ Supporting Information

The Supporting Information is available free of charge at https://pubs.acs.org/doi/10.1021/acsomega.1c01550.

ELF, CDD, and Bader charge of the $\text{Zn}_{37}\text{Se}_{20}\text{H}_{68}$ cluster; optimized structures, PDOS, and average bond lengths of modified ZnSe clusters; and absorption spectra of $\text{Zn}_{37}\text{Se}_{20}\text{H}_{68}$ and ZnSe MSC-299 (PDF)

■ AUTHOR INFORMATION

Corresponding Authors

Gao-Lei Hou − *Quantum Solid-State Physics, Department of Physics and Astronomy, KU Leuven, 3001 Leuven, Belgium;* ⓞ orcid.org/0000-0003-1196-2777; Email: gaolei.hou@kuleuven.be, chemglhou@gmail.com

Meng Zhang − *Institute of Atomic and Molecular Physics, Sichuan University, Chengdu, Sichuan 610065, P. R. China;* ⓞ orcid.org/0000-0002-2852-2527; Email: mengzhang@scu.edu.cn

Kui Yu − *Institute of Atomic and Molecular Physics, Sichuan University, Chengdu, Sichuan 610065, P. R. China; Engineering Research Center in Biomaterials, Sichuan University, Chengdu, Sichuan 610065, P. R. China; State Key Laboratory of Polymer Materials Engineering, Sichuan University, Chengdu, Sichuan 610065, P. R. China;* ⓞ orcid.org/0000-0003-0349-2680; Email: kuiyu@scu.edu.cn

Authors

Xiaolin Wang − *Institute of Atomic and Molecular Physics, Sichuan University, Chengdu, Sichuan 610065, P. R. China*

Yongcheng Zhu − *Institute of Atomic and Molecular Physics, Sichuan University, Chengdu, Sichuan 610065, P. R. China*

Mei Liu − *Institute of Atomic and Molecular Physics, Sichuan University, Chengdu, Sichuan 610065, P. R. China*

Gang Jiang − *Institute of Atomic and Molecular Physics, Sichuan University, Chengdu, Sichuan 610065, P. R. China;* ⓞ orcid.org/0000-0002-9385-0519

Complete contact information is available at:
https://pubs.acs.org/10.1021/acsomega.1c01550

Notes

The authors declare no competing financial interest.

■ REFERENCES

(1) Díaz, S. A.; Gillanders, F.; Jares-Erijman, E. A.; Jovin, T. M. Photoswitchable Semiconductor Nanocrystals with Self-Regulating Photochromic Forster Resonance Energy Transfer Acceptors. *Nat. Commun.* **2015**, *6*, No. 6036.

(2) Pimachev, A.; Dahnovsky, Y. Optical and Magnetic Properties of PbS Nanocrystals Doped by Manganese Impurities. *J. Phys. Chem. C* **2015**, *119*, 16941−16946.

(3) Ma, S.; Fei, S.; Huang, L.; Forrey, R. C.; Cheng, H. Tuning the Catalytic Activity of Pd_xNi_y (X+Y= 6) Bimetallic Clusters for Hydrogen Dissociative Chemisorption and Desorption. *ACS Omega* **2019**, *4*, 12498−12504.

(4) Fischer, S. A.; Crotty, A. M.; Kilina, S. V.; Ivanov, S. A.; Tretiak, S. Passivating Ligand and Solvent Contributions to the Electronic Properties of Semiconductor Nanocrystals. *Nanoscale* **2012**, *4*, 904−914.

(5) Burgos, J. C.; Mejía, S. M.; Metha, G. F. Effect of Charge and Phosphine Ligands on the Electronic Structure of the Au_8 Cluster. *ACS Omega* **2019**, *4*, 9169−9180.

(6) Del Ben, M.; Havenith, R. W. A.; Broer, R.; Stener, M. Density Functional Study on the Morphology and Photoabsorption of CdSe Nanoclusters. *J. Phys. Chem. C* **2011**, *115*, 16782−16796.

(7) Datta, S.; Kabir, M.; Saha-Dasgupta, T. Effects of Shape and Composition on the Properties of CdS Nanocrystals. *Phys. Rev. B* **2012**, *86*, No. 115307.

(8) Cohn, A. W.; Schimpf, A. M.; Gunthardt, C. E.; Gamelin, D. R. Size-Dependent Trap-Assisted Auger Recombination in Semiconductor Nanocrystals. *Nano Lett* **2013**, *13*, 1810−1815.

(9) Hori, Y.; Kano, S.; Sugimoto, H.; Imakita, K.; Fujii, M. Size-Dependence of Acceptor and Donor Levels of Boron and Phosphorus Codoped Colloidal Silicon Nanocrystals. *Nano Lett.* **2016**, *16*, 2615−2620.

(10) Krishnamurthi, P.; Raju, Y.; Khambhaty, Y.; Manoharan, P. T. Zinc Oxide-Supported Copper Clusters with High Biocidal Efficacy for Escherichia coli and Bacillus cereus. *ACS Omega* **2017**, *2*, 2524−2535.

(11) Kim, J.-Y.; Yang, J.; Yu, J. H.; Baek, W.; Lee, C.-H.; Son, H. J.; Hyeon, T.; Ko, M. J. Highly Efficient Copper-Indium-Selenide Quantum Dot Solar Cells: Suppression of Carrier Recombination by Controlled ZnS Overlayers. *ACS Nano* **2015**, *9*, 11286−11295.

(12) Heo, J. H.; Jang, M. H.; Lee, M. H.; Shin, D. H.; Kim, D. H.; Moon, S. H.; Kim, S. W.; Park, B. J.; Im, S. H. High-Performance Solid-State PbS Quantum Dot-Sensitized Solar Cells Prepared by Introduction of Hybrid Perovskite Interlayer. *ACS Appl. Mater. Interfaces* **2017**, *9*, 41104−41110.

(13) Kim, W. D.; Kim, J. H.; Lee, S.; Lee, S.; Woo, J. Y.; Lee, K.; Chae, W. S.; Jeong, S.; Bae, W. K.; McGuire, J. A.; Moon, J. H.; Jeong, M. S.; Lee, D. C. Role of Surface States in Photocatalysis: Study of Chlorine-Passivated CdSe Nanocrystals for Photocatalytic Hydrogen Generation. *Chem. Mater.* **2016**, *28*, 962−968.

(14) Zhang, J.; Hao, X.; Rowell, N.; Kreouzis, T.; Han, S.; Fan, H.; Zhang, C.; Hu, C.; Zhang, M.; Yu, K. Individual Pathways in the Formation of Magic-Size Clusters and Conventional Quantum Dots. *J. Phys. Chem. Lett.* **2018**, *9*, 3660−3666.

(15) Chen, M.; Luan, C.; Zhang, M.; Rowell, N.; Willis, M.; Zhang, C.; Wang, S.; Zhu, X.; Fan, H.; Huang, W.; Yu, K.; Liang, B. Evolution

of CdTe Magic-Size Clusters with Single Absorption Doublet Assisted by Adding Small Molecules during Prenucleation. *J. Phys. Chem. Lett.* **2020**, *11*, 2230−2240.

(16) Kudera, S.; Zanella, M.; Giannini, C.; Rizzo, A.; Li, Y.; Gigli, G.; Cingolani, R.; Ciccarella, G.; Spahl, W.; Parak, W. J.; Manna, L. Sequential Growth of Magic-Size CdSe Nanocrystals. *Adv. Mater.* **2007**, *19*, 548−552.

(17) McBride, J. R.; Dukes, A. D., III; Schreuder, M. A.; Rosenthal, S. J. On Ultrasmall Nanocrystals. *Chem. Phys. Lett.* **2010**, *498*, 1−9.

(18) Zhang, J.; Rowland, C.; Liu, Y.; Xiong, H.; Kwon, S.; Shevchenko, E.; Schaller, R. D.; Prakapenka, V. B.; Tkachev, S.; Rajh, T. Evolution of Self-Assembled ZnTe Magic-Sized Nanoclusters. *J. Am. Chem. Soc.* **2015**, *137*, 742−749.

(19) Kasuya, A.; Sivamohan, R.; Barnakov, Y. A.; Dmitruk, I. M.; Nirasawa, T.; Romanyuk, V. R.; Kumar, V.; Mamykin, S. V.; Tohji, K.; Jeyadevan, B.; Shinoda, K.; Kudo, T.; Terasaki, O.; Liu, Z.; Belosludov, R. V.; Sundararajan, V.; Kawazoe, Y. Ultra-Stable Nanoparticles of CdSe Revealed from Mass Spectrometry. *Nat. Mater.* **2004**, *3*, 99−102.

(20) Beecher, A. N.; Yang, X.; Palmer, J. H.; LaGrassa, A. L.; Juhas, P.; Billinge, S. J. L.; Owen, J. S. Atomic Structures and Gram Scale Synthesis of Three Tetrahedral Quantum Dots. *J. Am. Chem. Soc.* **2014**, *136*, 10645−10653.

(21) Gary, D. C.; Flowers, S. E.; Kaminsky, W.; Petrone, A.; Li, X.; Cossairt, B. M. Single-Crystal and Electronic Structure of a 1.3 nm Indium Phosphide Nanocluster. *J. Am. Chem. Soc.* **2016**, *138*, 1510−1513.

(22) Williamson, C. B.; Nevers, D. R.; Nelson, A.; Hadar, I.; Banin, U.; Hanrath, T.; Robinson, R. D. Chemically Reversible Isomerization of Inorganic Clusters. *Science* **2019**, *363*, 731−715.

(23) Tan, L.; Misquitta, A.; Sapelkin, A.; Fang, L.; Wilson, R. M.; Keeble, D. S.; Zhang, B.; Zhu, T.; Riehle, F. S.; Han, S.; Yu, K.; Dove, M. T. X-Ray Total Scattering Study of Regular and Magic-Size Nanoclusters of Cadmium Sulphide. *Nanoscale* **2019**, *11*, 21900.

(24) Wang, L.; Hui, J.; Tang, J.; Rowell, N.; Zhang, B.; Zhu, T.; Zhang, M.; Hao, X.; Fan, H.; Zeng, J.; Han, S.; Yu, K. Precursor Self-Assembly Identified as a General Pathway for Colloidal Semiconductor Magic-Size Clusters. *Adv. Sci.* **2018**, *5*, No. 1800632.

(25) Gary, D. C.; Petrone, A.; Li, X.; Cossairt, B. M. Investigating the Role of Amine in InP Nanocrystal Synthesis: Destabilizing Cluster Intermediates by Z-Type Ligand Displacement. *Chem. Commun.* **2017**, *53*, 161−164.

(26) Stein, J. L.; Steimle, M. I.; Terban, M. W.; Petrone, A.; Billinge, S. J. L.; Li, X.; Cossairt, B. M. Cation Exchange Induced Transformation of InP Magic-Sized Clusters. *Chem. Mater.* **2017**, *29*, 7984−7992.

(27) Friedfeld, M. R.; Stein, J. L.; Ritchhart, A.; Cossairt, B. M. Conversion Reactions of Atomically Precise Semiconductor Clusters. *Acc. Chem. Res.* **2018**, *51*, 2803−2810.

(28) Yu, M.; Fernando, G. W.; Li, R.; Papadimitrakopoulos, F.; Shi, N.; Ramprasad, R. First Principles Study of CdSe Quantum Dots: Stability, Surface Unsaturations, and Experimental Validation. *Appl. Phys. Lett.* **2006**, *88*, No. 231910.

(29) Zhao, Q.; Kulik, H. J. Electronic Structure Origins of Surface-Dependent Growth in III−V Quantum Dots. *Chem. Mater.* **2018**, *30*, 7154−7165.

(30) Datta, S.; Kabir, M.; Saha-Dasgupta, T.; Sarma, D. D. First-Principles Study of Structural Stability and Electronic Structure of CdS Nanoclusters. *J. Phys. Chem. C* **2008**, *112*, 8206−8214.

(31) Zhao, F. A.; Xiao, H. Y.; Bai, X. M.; Zu, X. T. Effects of Ag Doping on the Electronic and Optical Properties of CdSe Quantum Dots. *Phys. Chem. Chem. Phys.* **2019**, *21*, 16108−16119.

(32) Deng, H.; Li, S.-S.; Li, J.; Wei, S.-H. Effect of Hydrogen Passivation on the Electronic Structure of Ionic Semiconductor Nanostructures. *Phys. Rev. B* **2013**, *85*, No. 195328.

(33) Azpiroz, J. M.; Infante, I.; Lopez, X.; Ugalde, J. M.; Angelis, F. D. A First-Principles Study of II−VI (II = Zn; VI = O, S, Se, Te) Semiconductor Nanostructures. *J. Mater. Chem.* **2012**, *22*, 21453−21465.

(34) Jin, S.; Chen, B.; Kuang, X.; Lu, C.; Gutsev, G. L. Structural Evolution and Electronic Properties of Medium-Sized Boron Clusters Doped with Scandium. *J. Phys.: Condens. Matter* **2019**, *31*, No. 485302.

(35) Granja-DelRío, A.; Abdulhussein, H. A.; Johnston, R. L. DFT-Based Global Optimization of Sub-nanometer Ni−Pd Clusters. *J. Phys. Chem. C* **2019**, *123*, 26583−26596.

(36) Azpiroz, J. M.; Matxain, J. M.; Infante, I.; Lopez, X.; Ugalde, J. M. A DFT/TDDFT Study on the Optoelectronic Properties of the Amine-Capped Magic (CdSe)$_{13}$ Nanocluster. *Phys. Chem. Chem. Phys.* **2013**, *15*, 10996−11005.

(37) Kresse, G.; Hafner, J. Ab Initio Molecular Dynamics for Liquid Metals. *Phys. Rev. B* **1993**, *47*, 558−561.

(38) Kresse, G.; Furthmüller, J. Efficient Iterative Schemes for Ab Initio Total-Energy Calculations Using a Plane-Wave Basis Set. *Phys. Rev. B* **1996**, *54*, 11169−11186.

(39) te Velde, G.; Bickelhaupt, F. M.; Baerends, E. J.; Fonseca Guerra, C.; van Gisbergen, S. J. A.; Snijders, J. G.; Ziegler, T. Chemistry with ADF. *J. Comput. Chem.* **2001**, *22*, 931−967.

(40) Frisch, M. J.; Trucks, G. W.; Schlegel, H. B.; Scuseria, G. E.; Robb, M. A.; Cheeseman, J. R.; Scalmani, G.; Barone, V.; Mennucci, B.; Petersson, G. A.; Nakatsuji, H.; Caricato, M.; Li, X.; Hratchian, H. P.; Izmaylov, A. F.; Bloino, J.; Zheng, G.; Sonnenberg, J. L.; Hada, M.; Ehara, M.; Toyota, K.; Fukuda, R.; Hasegawa, J.; Ishida, M.; Nakajima, T.; Honda, Y.; Kitao, O.; Nakai, H.; Vreven, T.; Montgomery, J. A., Jr; Peralta, J. E.; Ogliaro, F.; Bearpark, M.; Heyd, J. J.; Brothers, E.; Kudin, K. N.; Staroverov, V. N.; Kobayashi, R.; Normand, J.; Raghavachari, K.; Rendell, A.; Burant, J. C.; Iyengar, S. S.; Tomasi, J.; Cossi, M.; Rega, N.; Millam, J. M.; Klene, M.; Knox, J. E.; Cross, J. B.; Bakken, V.; Adamo, C.; Jaramillo, J.; Gomperts, R.; Stratmann, R. E.; Yazyev, O.; Austin, A. J.; Cammi, R.; Pomelli, C.; Ochterski, J. W.; Martin, R. L.; Morokuma, K.; Zakrzewski, V. G.; Voth, G. A.; Salvador, P.; Dannenberg, J. J.; Dapprich, S.; Daniels, A. D.; Farkas, O.; Foresman, J. B.; Ortiz, J. V.; Cioslowski, J.; Fox, D. J. *Gaussian 09*, revision A.02; Gaussian, Inc.: Wallingford, CT, 2009.

(41) Shiraishi, K. A New Slab Model Approach for Electronic Structure Calculation of Polar Semiconductor Surface. *J. Phys. Soc. Jpn.* **1990**, *59*, 3455−3458.

(42) Huang, X.; Lindgren, E.; Chelikowsky, J. R. Surface Passivation Method for Semiconductor Nanostructures. *Phys. Rev. B* **2005**, *71*, No. 165328.

(43) Li, J.; Wang, L.-W. Band-Structure-Corrected Local Density Approximation Study of Semiconductor Quantum Dots and Wires. *Phys. Rev. B* **2005**, *72*, No. 125325.

(44) Voznyy, O.; Mokkath, J. H.; Jain, A.; Sargent, E. H.; Schwingenschlogl, U. Computational Study of Magic-Size CdSe Clusters with Complementary Passivation by Carboxylic and Amine Ligands. *J. Phys. Chem. C* **2016**, *120*, 10015−10019.

(45) Deng, H.-X.; Li, S.-S.; Li, J.; Wei, S.-H. Effect of Hydrogen Passivation on the Electronic Structure of Ionic Semiconductor Nanostructures. *Phys. Rev. B* **2012**, *85*, No. 195328.

(46) Nanavati, S. P.; Sundararajan, V.; Mahamuni, S.; Kumar, V.; Ghaisas, S. V. Optical Properties of Zinc Selenide Clusters from First-Principles Calculations. *Phys. Rev. B* **2009**, *80*, No. 245417.

(47) Blöchl, P. E. Projector Augmented-Wave Method. *Phys. Rev. B* **1994**, *50*, 17953−17979.

(48) Kilina, S.; Ivanov, S.; Tretiak, S. Effect of Surface Ligands on Optical and Electronic Spectra of Semiconductor Nanoclusters. *J. Am. Chem. Soc.* **2009**, *131*, 7717−7726.

(49) Kamisaka, H.; Kilina, S. V.; Yamashita, K.; Prezhdo, O. V. Ab Initio Study of Temperature and Pressure Dependence of Energy and Phonon-Induced Dephasing of Electronic Excitations in CdSe and PbSe Quantum Dots†. *J. Phys. Chem. C* **2008**, *112*, 7800−7808.

(50) Shanavas, K. V.; Sharma, S. M.; Dasgupta, I.; Nag, A.; Hazarika, A.; Sarma, D. D. First-Principles Study of the Effect of Organic Ligands on the Crystal Structure of CdS Nanoparticles. *J. Phys. Chem. C* **2012**, *116*, 6507−6511.

(51) Deák, P.; Aradi, B.; Frauenheim, T.; Janzén, E.; Gali, A. Accurate Defect Levels Obtained from the HSE06 Range-Separated Hybrid Functional. *Phys. Rev. B* **2010**, *81*, No. 153203.

(52) Heyd, J.; Scuseria, G. E. Hybrid Functionals Based on a Screened Coulomb Potential. *J. Chem. Phys.* **2003**, *118*, 8207−8215.

(53) Cho, E.; Jang, H.; Lee, J.; Jang, E. Modeling on the Size Dependent Properties of InP Quantum Dots: A Hybrid Functional Study. *Nanotechnology* **2013**, *24*, No. 215201.

(54) Burdett, J. K.; McCormick, T. A. Electron Localization in Molecules and Solids: The Meaning of ELF. *J. Phys. Chem. A* **1998**, *102*, 6366−6372.

(55) Becke, A. D.; Edgecombe, K. E. A Simple Measure of Electron Localization in Atomic and Molecular-Systems. *J. Chem. Phys.* **1990**, *92*, 5397−5403.

(56) Togo, A.; Tanaka, I. First Principles Phonon Calculations in Materials Science. *Scr. Mater.* **2015**, *108*, 1−5.

(57) Tang, W.; Sanville, E.; Henkelman, G. A Grid-Based Bader Analysis Algorithm without Lattice Bias. *J. Phys.: Condens. Matter* **2009**, *21*, No. 084204.

(58) Sanville, E.; Kenny, S. D.; Smith, R.; Henkelman, G. Improved grid-based algorithm for Bader charge allocation. *J. Comput. Chem.* **2007**, *28*, 899−908.